coumarin 6, - labeled polylactic acid particles of the size about 1 μm were prepared by adding the mixture of the particles and the coumarin 6 in Ch_2Cl_2 into the 0.25% polyvinyl alcohol aqueous solution under ultrasonication. The fluorescent image from each organ was obtained. The distribution inside the organ was also inspected by elemental mapping using energy dispersive X-ray spectroscopy (EDS) installed to SEM.

3. Visualization in the Tissue and Intracellular Level. Histological and ultrastructural investigations were carried out by optical and transmission electron microscopy (OM, TEM) for the specimens prepared by ordinary process [6].

Results

1. XSAM elemental detection. Fig.1 is the XSAM elemental analysis of spleen after 10 days of oral administration of 30nm TiO_2 particles to a mouse. Although the peak height is small compared with Fe-Kα peaks around 6.5keV and those of incident X-ray beam from Rh target below 4keV, Ti-Kα peak undoubtedly exists. This confirms the phenomenon that nanoparticles were taken into the internal body through digestion system. The uptake of 30nm TiO_2 particles through the respiratory system and diffusion into the whole body was also confirmed.

2. Microscopic observation of fluorescence-labeled particles. Fig.2 is the fluorescent microscopic image of spleen at 1 week after injection of 1 μm particles of coumarin 6-labeled polylactic acid to caudal vein. Fluorescent spots are visible to be distributed all over the spleen. Judging from the spot size around 1 μm, each spot looks corresponding to a single particle. The particles of polylactic acid seem to have little tendency to coagulate. The distribution of fluorescent spots are also found in the lung and livers. They might diffuse rather dispersedly and result in being trapped in the relevant organs.

3. MRI imaging of magnetic nanoparticles. Fig.3 is MRI image before and after injection of 11 nm magnetite Fe_3O_4 particles to caudal vein. These particles are fabricated for the optimum performance of hyperthermia therapy to cancer. Due to the contrast darkened by magnetism of Fe_3O_4 particles, the comparison of images before and after injection verifies the contrast change occurred in the liver, indicating the enrichment of Fe_3O_4 particles. The similar change was observed in the spleen and kidney.

4. XSAM elemental mapping. Fig.4 is the change of XSAM Ti mappings of internal distribution of 30 nm TiO_2 particles in the body of mouse with time after injection to caudal vein. TiO_2 nanoparticles diffuse to the lung just after injection from caudal vein, then with time course to the liver and further to the spleen, which is not shown here. The following time sequence of XSAM Ti mapping shows the decrease in the lung and the increase in the liver. It takes longer time for the increase in the spleen.

Fig.5 is the XSAM Pt mapping of the lung, liver, spleen and kidney at 1 day after injection of 1 μm Pt particles to caudal vein. The Pt concentration is the highest in the spleen, followed by the liver.

5. Chemical analysis of particles contained in organs. Fig.6 shows the ICP-AES chemical analysis of total Pt content detected from each organ shown in Fig.5 at 1 day after injection. The Pt concentration in each organ was also analyzed and agreed with the results obtained by XSAM analysis of Fig.5. The total Pt content is the largest in the liver, then spleen and slight in the kidney. Although the concentration is the highest in the spleen, the total content is the largest in the liver because of the large volume.

Discussion

In the present study we used the plural methods based on the different principles to enable the visualization of internal diffusion of particles.

XSAM forms the convergent X-ray probe of 100 – 10 μm, irradiates the specimen, detects the emitted fluorescent characteristic X-ray and makes elemental mapping image as well as transmission X-ray image for the sectioned specimens. Visualization of distribution for the large

scale around 100 mm such as the full body size of rat (Fig.4) is possible in air with the high sensitivity of about 100 ppm and the spatial resolution of probe size100 – 10 μm. The comparison of XSAM mapping image (Fig.5) with the quantitative chemical analysis using ICP-AES (Fig.6) verifies the detectable concentration at 100 ppm level. This method could show the time sequence of particle diffusion from organ to organ [7].

MRI can perform the three-dimensional observation, make the horizontal or vertical image at any section as animal alive and trace the change with time using the same animal. However MRI utilizes the change of image contrast by magnetism, therefore the applicable particles are limited to the magnetic or magnetism-labeled materials. In the present study the 11 nm magnetite Fe_3O_4 particles fabricated for hyperthermia therapy against cancer were used. The results were more or less in agreement with those obtained by XSAM method.

Other than XSAM, we also used the Laser Ablation / Mass Spectroscopy Method, which analyzes mass by TOFMS (Time of Flight Type Mass Spectrometer) after the target is evaporated by laser irradiation and make two-dimensional distribution image of the desired mass. This is especially valuable for the materials composed of carbon as main constituent such as pure carbon of fullerenes, carbon nanotubes or carbon compounds of saccharides and proteins, since elemental analysis such as XSAM cannot distinguish these from tissue composed of C, N, O, H.

Conclusions

Particles cause different reaction to cell/tissue depending on their size [8,9]. This physical size effect is pronounced for less than 10 μm and causes stimulus by biological process of phagocytosis in cell and inflammation in tissue [1]. When the particle size becomes in the level of 50nm or less, they become less stimulative and the recognition by body defense system becomes weaker. The invasion of nanoparticles into the body and internal diffusion occurs for this range of particle size [10]. The present study could successfully make the visualization of internal diffusion of particles by different methods. The informations obtained here contribute to both risk assessement of nanoparticles and drug delivery path of DDS.

Acknowledgements

Research supported by Health and Laybour Sciences Research Grants in Research on Chemical Substance Assessment of Ministry of Health, Laybour and Welfare of Japan (H18-Chem-General-006).

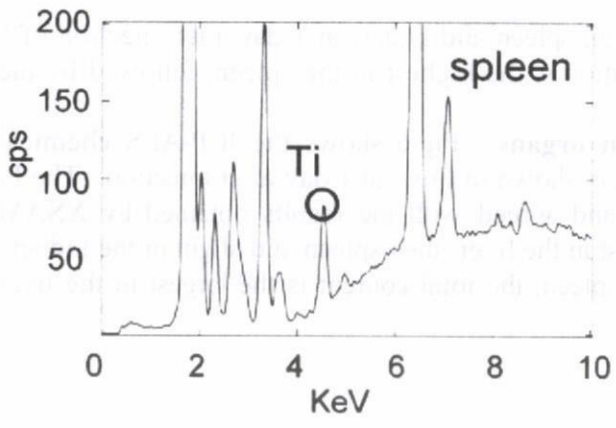

Fig.1 XSAM elemental analysis of spleen after 10 days of oral administration of 30nm TiO_2 particles

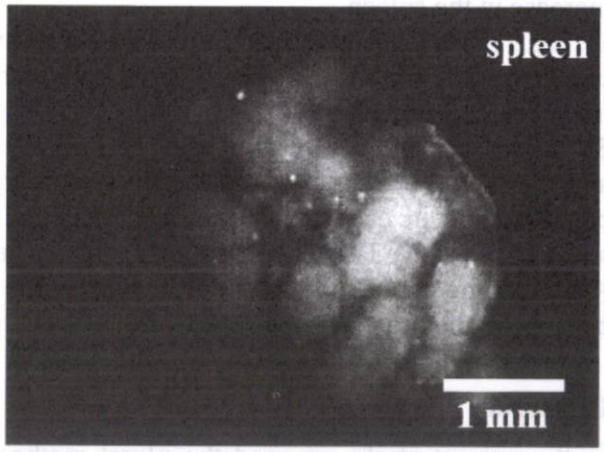

Fig.2 Fluorescent microscopic image of spleen at 1 week after injection of 1 μm particles of coumarin 6- labeled polylactic acid to caudal vein.

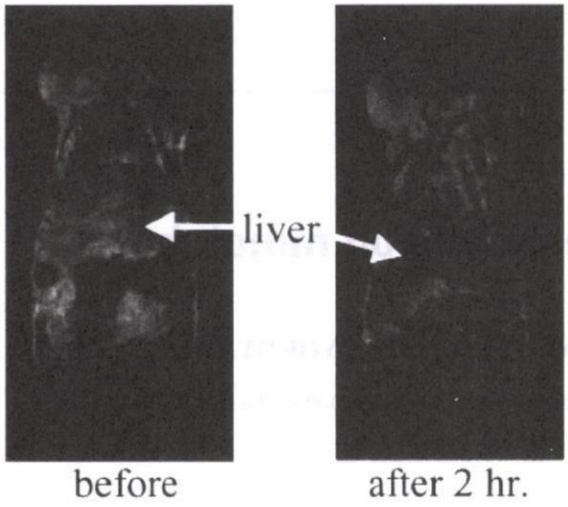

Fig.3 MRI image before and after injection of 11 nm Fe_3O_4 particles to caudal vein

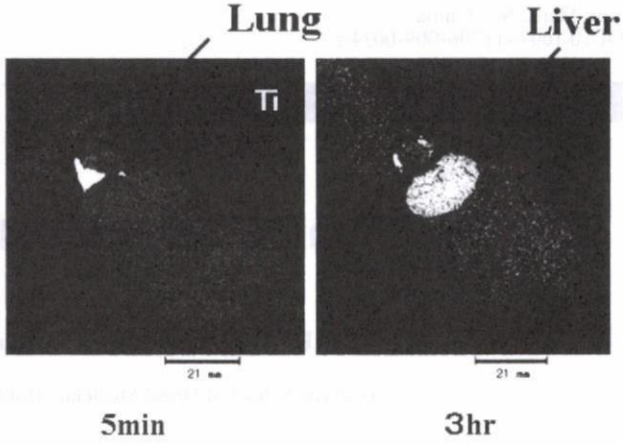

Fig.4 XSAM Ti mapping of internal distribution of 30 nm TiO_2 particles after injection to caudal vein

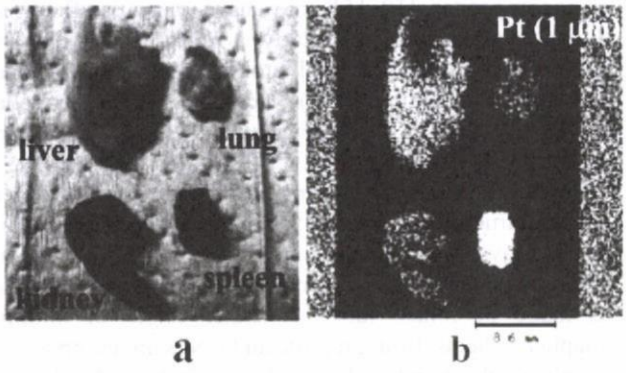

Fig.5 XSAM Pt mapping of each organ at 1 day after injection of 1 μm Pt particles to caudal vein.

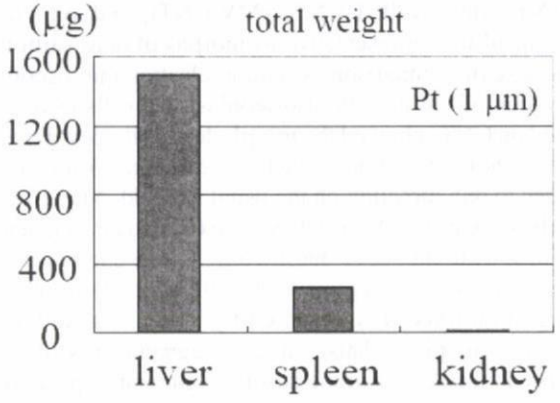

Fig.6 ICP-AES chemical analysis of Pt element contained in each organ shown in Fig.5

References

[1] F.Watari, K.Tamura, A.Yokoyama, K.Shibata, T.Akasaka, B.Fugetsu, K.Asakura, M.Uo, Y.Totsuka, Y.Sato, K.Tohji: Handbook of Biomineralization, Vol.3, Ed.E.Bauerlein, Wiley-VCH, Weinheim, p.127-144 (2007)

[2] M.Uo, F.Watari, A.Yokoyama, H.Matsuno, T.Kawasaki: Biomaterials 20(1999), 747-755

[3] M.Uo, M.Tanaka, F.Watari: J.Biomed.Mater.Res.Part B:Appl.Biomater. 70B(2004), 146-151

[4] M.Ushiro, K.Uno, T.Fujikawa, Y.Sato, K.Tohji, F.Watari, W.Chun, Y.Koike, K.Asakura: Phys. Rev. B 73, 144103/1-11(2006)

[5] Aoki N, Akasaka T, Watari F, Yokoyama A, *Dent.Mat.J.*, 26 (2007) 178-185

[6] A.Yokoyama, Y.Sato, Y.Nodasaka, S.Yamamoto, T.Kawasaki, M.Shindoh, T.Kohgo, T.Akasaka, M.Uo, F.Watari, K.Tohji: Nano Letters 5 (2005) , 157-161

[7] F.Watari, S.Abe, C.Koyama, A.Yokoyama, T.Akasaka, M.Uo, M.Matsuoka, Y.Totsuka, M.Esaki, M.Morita, T.Yonezawa: J.Cera.Soc.Jap., 116 (1) , 1-5, 2008

[8] R.Kumazawa, F.Watari, N.Takashi, Y.Tanimura, M.Uo, Y.Totsuka: Biomaterials 23(2002), 3757-3764

[9] K.Tamura, N.Takashi, R.Kumazawa, F.Watari, Y.Totsuka: Mat.Trans. 43(2002), 3052-3057

[10] F.Watari, S.Abe, K.Tamura, M.Uo, A.Yokoyama, Y.Totsuka: Bioceramics Vol.20 Part 1, (Key Engineering Materials Vols.361-363), Trans.Tech.Publ., p.95-98, 2007

Front. Mater. Sci. China
DOI 10.1007/s11706-009-0034-z

RESEARCH ARTICLE

Proliferation of osteoblast cells on nanotubes

F. WATARI (✉), T. AKASAKA, Xiaoming LI, M. UO, A. YOKOYAMA

Graduate School of Dental Medicine, Hokkaido University, Sapporo 060-8586, Japan

Abstract Carbon nanotubes (CNT) have a unique structure and feature. In the present study, cell proliferation was performed on the scaffolds of single-walled CNTs (SWCNT), multiwalled CNTs (MWCNT), and on graphite, one of the representative isomorphs of pure carbon, for the sake of comparison. Scanning electron microscopy observation of the growth of osteoblast-like cells (Saos2) cultured on CNTs showed the morphology fully developed for the whole direction, which is different from that extended to one direction on the usual scaffold. Numerous filopodia were grown from cell edge, extended far long and combined with the CNT meshwork. CNTs showed the affinity for collagen and proteins. Proliferated cell numbers are largest on SWCNTs, followed by MWCNTs, and are very low on graphite. This is in good agreement with the sequence in the results of the adsorbed amount of proteins and expression of alkaline phosphatase activity for these scaffolds. The adsorption of proteins would be one of the most influential factors to make a contrast difference in cell attachment and proliferation between graphite and CNTs, both of which are isomorphs of carbon and composed of similar graphene sheet crystal structure. In addition, the nanosize meshwork structure with large porosity is another property responsible for the excellent cell adhesion and growth on CNTs. CNTs could be the favorable materials for biomedical applications.

Keywords carbon nanotube, scaffold, osteoblast, regeneration, nanomaterial

1 Introduction: Two isomorphs of carbon–graphite and CNT

Carbon nanotubes (CNT) [1,2] have attracted much attention due to their unique feature in the application in the electronic and chemical fields. Recent derivatives of CNTs with different structures and compositions have been synthesized and discovered [3]. Nanomaterials [2–9] and nanocomposites [10–15] may have various effects on living organisms. In this study, a fundamental study for biomedical application, cell proliferation was performed on various nanotubes (NT), including (1) single-walled CNTs (SWCNT), (2) multiwalled CNTs (MWCNT), and on graphite, an isomorph of CNT, as a comparison.

Figure 1 shows the schematic figures of two different crystal structures of carbon: graphite and CNT. Graphite has the layer-by-layer laminated structure of flat graphene sheets, composed of C six-membered rings, whereas CNT is made of folded tubes of either single or multiple graphene sheets. Both graphite and CNTs are composed of graphene sheet and hydrophorbic characters. As element, carbon (C) would be bioinert. Graphite is used as an artificial heart valve due to its antithrombogenicity for biomedical applications. There have not been so many studies on CNTs, about their biological effects and biomedical applications [2,3,7–9,15–24]. In the present study, to evaluate the properties of CNTs in the aspects of biomedical nature, cell proliferation was performed on the scaffolds of SWCNTs and MWCNTs, and compared with that on graphite. Their features and the difference of properties are then discussed.

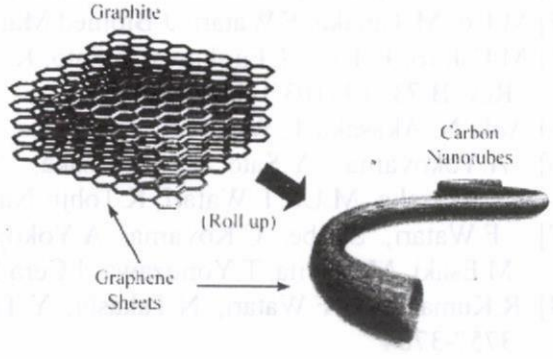

Fig. 1 Schematic figures of two different crystal structures of carbon, graphite and CNT

Received December 3, 2008; accepted January 9, 2009

E-mail: watari@den.hokudai.ac.jp

2 Materials and methods

SWCNTs of 0.9–1.5 nm diameter and 2–3 μm length synthesized by the arc discharge method with a purity of 90% (Meijo Nano Carbon Co., LTD.) and MWCNTs of 5–20 nm diameter and 20–40 μm length synthesized by the chemical vapor deposition technique with a purity of 98% (NanoLab Inc., MA USA) were used. In some cases CNTs were purified by the removal of metal particle catalysts such as Ni, Fe using acid agents and amorphous carbon by heating in air. By these treatments [3,7] CNTs got some hydrophilicity. Various NT scaffolds were made by vacuum filtration of the dispersed NT slurry onto porous polycarbonate membranes (PC) [18–20].

Human osteoblast-like cells (Saos2) were used for cell culture on NTs. Cell culture was done in Dulbecco's modified Eagle's medium (SIGMA) with 10% fetal bovine serum (Biowest) in the usual process. The morphology of cells was observed by optical microscopy, confocal laser scanning microscopy, and scanning electron microscopy (SEM). The number of cells was counted from the SEM micrographs of those attached to each scaffold, since the detachment of cells from scaffold by tripsin could not be applied for CNT scaffolds. The adsorbed amount of proteins on each scaffold was measured by the BCA method after immersion in the cell culture medium for 24 h. Alkaline phosphatase (ALP) activity was measured with LabAssay ALP (Wako, Japan) for the cells cultured on each scaffold [18].

3 Results

3.1 Cell proliferation on graphite and CNTs

Figure 2 shows the SEM image of osteoblast-like Saos2 cells cultured on graphite and MWCNT for 7 d. Very few cells were attached on graphite, while many cells were on CNTs.

Figure 3 shows the number of Saos2 cells cultured on the scaffolds of polycarbonate, graphite, MWCNT, and SWCNT for 3 and 7 d [18]. The cell numbers were increased with culture time. However, cell number remained nearly null on graphite. The cell numbers were largest on SWCNTs among the four scaffolds, followed by MWCNTs.

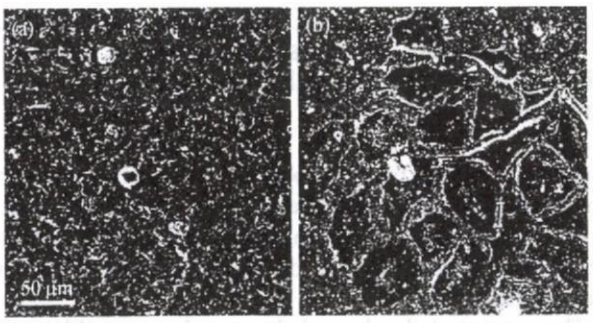

Fig. 2 SEM image of osteoblast-like Saos2 cells cultured on **(a)** graphite and **(b)** MWCNT scaffolds for 7 d

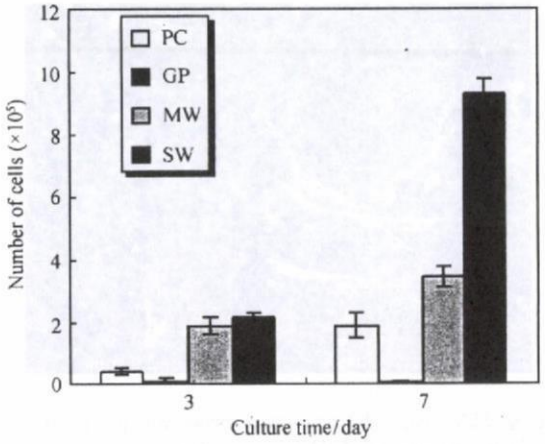

Fig. 3 Number of Saos2 cells cultured on the scaffolds of polycarbonate, graphite, MWCNT, and SWCNT for 3 and 7 d [18]

Osteoblast-like cells are usually grown in a spindle shape ~~as in Fig. 2(a)~~. On CNT scaffold, cells are grown fully to the whole direction [Fig. 2(b)] [18–20]. Figure 4 shows the SEM observation of filopodia grown from the periphery of osteoblast-like cells on the polycarbonate and MWCNT scaffolds. It is noted that numerous filopodia are extended far from cell edge onto CNTs (Fig. 5). They are mechanically combined with CNT meshwork. When tripsin, usually used to detach cells for cell number counting, was applied, cells were going to detach and float up, but could not be separated from the scaffold due to the mechanical binding of filopodia with CNTs. These results show the high cell adhesiveness of CNTs.

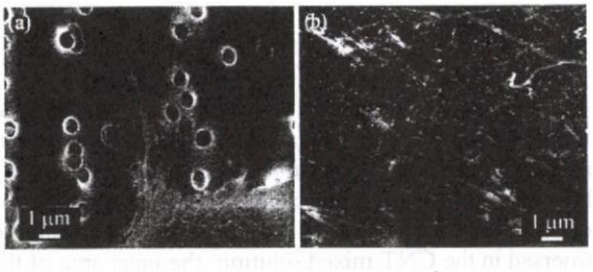

Fig. 4 SEM observation of filopodia grown from the periphery of osteoblast-like cells on **(a)** polycarbonate and **(b)** MWCNT scaffolds

3.2 Biomimetic coating of hydroxyapatite on CNT

Figure 6 is the SEM image of CNTs after immersion in simulated body fluid (SBF) for 2 weeks. Apatite was precipitated on CNT agglomeration [21,22]. This kind of

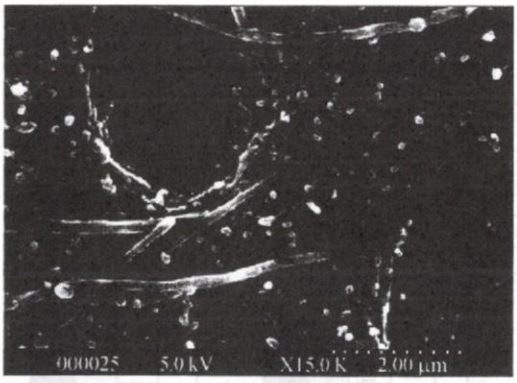

Fig. 5 SEM image of dentin surface etched with phosphoric acid after being immersed in CNT mixed solution

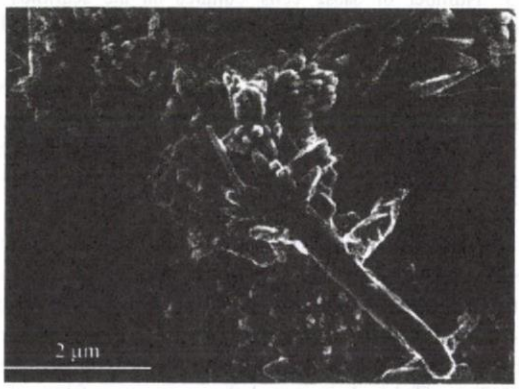

Fig. 6 SEM image of CNTs after immersion in SBF for 2 weeks

precipitation of calcium phosphate by immersion in SBF is known as the so-called biomimetic coating, which occurs typically on titanium (Ti) to form the calcium phosphate layer on its surface. This process is one of the reasons for the excellent biocompatibility of Ti, which may also be the case for CNTs.

3.3 Adsorption of CNTs onto collagen fibrils on dentin

In the treatment of dentistry for composite resin restoration, teeth are pretreated with an acid etching agent such as phosphoric acid and citric acid to enhance the interlocking effect between teeth and composite resin. When the sectioned teeth are pretreated with acid etching agent and immersed in the CNT mixed solution, the inner area of the teeth, dentin, looks black, while enamel remains white. Without acid etching dentin remains white. SEM observation reveals the adsorption of CNTs on dentin and no adsorption on enamel. Figure 5 is the enlarged SEM image of dentin surface etched with phosphoric acid after being immersed in CNT mixed solution. Dentinal tubules are observed. Collagen fibrils are exposed all over the dentin surface due to demineralization by acid etching. CNTs (long fibers) are found to be adsorbed to collagen fibrils exposed on dentin surface by acid etching. The fact that CNTs are adsorbed only on dentin but not on enamel suggests the nonspecific affinity of CNTs to proteins.

3.4 Adsorption of proteins on CNTs

Figure 7 shows the adsorbed amount of proteins on the scaffolds of polycarbonate, graphite, MWCNT, and SWCNT when immersed in the cell culture medium for 24 h [18]. The adsorbed protein amount level is very low for graphite, and is highest for SWCNT, followed by MWCNT.

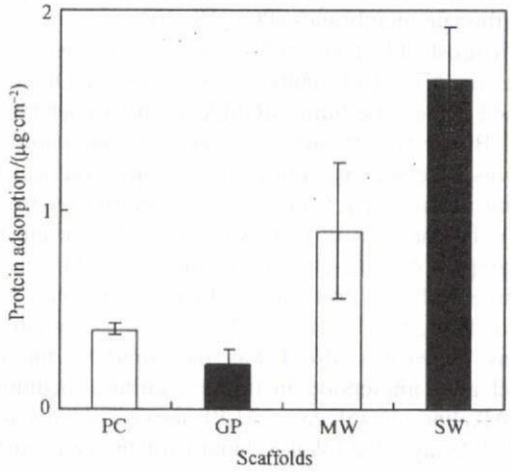

Fig. 7 Adsorbed amount of proteins on the scaffolds of polycarbonate (PC), graphite (GP), MWCNT (MW), and SWCNT (SW) in cell culture medium after 24 h [18]

3.5 ALP activity of osteoblast-like cells on CNTs

Figure 8 is the expression of total ALP activity from osteoblast-like cells cultured on the scaffolds of polycarbonate, graphite, MWCNT, and SWCNT for 3 and 7 d [18]. The degree of expression increases with culture time. It remains very low for graphite, while it increases remarkably in CNTs, the most in SWCNTs, then MWCNTs.

4 Discussion: Factors that make a difference in biological effect between graphite and CNTs

Graphite and CNTs are isomorphs of carbon and are composed of similar graphene sheet crystal structures (Fig. 1). Although the element carbon is bioinert, graphite and CNTs make a contrast difference in cell attachment and proliferation.

The present study showed the very low osteoblast cell attachment and proliferation on graphite. This is one of the properties inducing antithrombogenicity, which is utilized

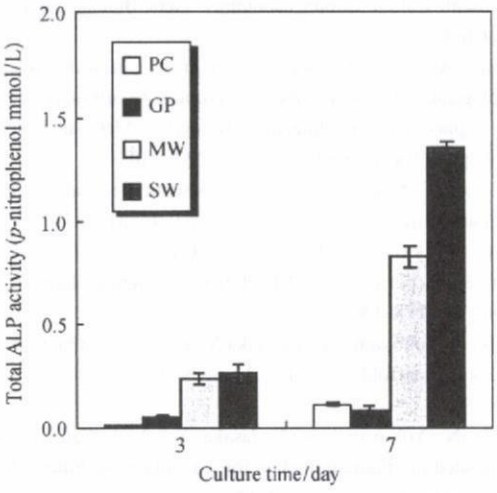

Fig. 8 Expression of total ALP activity from Saos2 cells cultured on the scaffolds of polycarbonate, graphite, MWCNT, and SWCNT, for 3 and 7 d [18]

for the application in artificial heart valve. By contrast, cell numbers and growth cultured on CNTs showed the characteristic behavior. Cell numbers proliferated on CNTs are much larger (Fig. 3). Osteoblast-like cell is usually grown in a spindle shape. On CNT scaffolds, cells are grown fully to the whole direction with numerous fine filopodia extended far from cell edge (Fig. 4) [18–20], which are mechanically combined with CNT meshwork. When tripsin, usually used to detach cells for cell number counting, was applied, cells were going to detach and float up, but could not be separated from the scaffold due to the mechanical binding of filopodia with CNTs [18]. All these results suggest the very good compatibility of CNTs to cells.

When CNTs are immersed in SBF, hydroxyapatite is precipitated [21,22]. This ~~work proves~~ the biocompatibility of CNTs as in the case of Ti.

However, one of the most influential factors to make a contrast difference in cell attachment and proliferation between graphite and CNTs would be the nonspecific affinity of CNTs to collagen, proteins, and also saccharides. Proliferated cell numbers are the largest on SWCNTs, followed by MWCNTs, and are very low on graphite (Fig. 3). This is in good agreement with the sequence in the results of the adsorbed amount of proteins (Fig. 7) and expression of ALP activity (Fig. 8). The culture medium contains various proteins including growth factors, which may affect the cell functions such as ALP activity, one of the markers of capability of new bone formation of osteoblasts. Therefore, the adsorption of proteins provides the favorable conditions to cells in the chemical or material aspects [18,23,24].

Another factor is the structural view point. Although CNTs generally have the tendency to agglomerate and form bundles, the wavy, fibrous agglomeration makes still a nano-meshwork conformation with a large porosity where cells can take nutrient elements or growth factors easily. In addition, the nanosize diameter of CNT fibers, a few to several tens nanometers, is close to that of filopodia of cells, which is about 100 nm. ~~And it~~ seems easy for the end of filopodia to interact with the CNT network. Tripsin is generally used for the detachment of cells from scaffold. On CNT scaffolds, however, cells cannot separate because of the mechanical binding of filopodia with the CNT network, which demonstrates the good cell adhesive properties of CNTs. All these would work for the excellent cell adhesion and growth on CNTs. Thus, CNTs could be the favorable materials for biomedical applications.

5 Conclusions

Graphite and CNTs, isomorphs of carbon composed of a similar graphene sheet crystal structure, showed a contrasting feature in cell attachment and proliferation, which is very low on graphite and excellent on CNTs. The affinity of CNTs to proteins leads to the high adsorption of proteins including growth factors in cell culture, which is responsible for excellent cell adhesion, growth, and its functional expression of ALP activity. In addition, the nano-meshwork structure of CNT agglomeration contributes physically to the favorite conditions for cell attachment. CNTs would work as scaffolds with the characteristic features.

Acknowledgements Research supported by Health and Labour Sciences Research Grants in Research on Chemical Substance Assessment of Ministry of Health, Labour and Welfare of Japan (H18-Chem-General-006).

References

1. Ushiro M, Uno K, Fujikawa T, et al. X-ray absorption fine structure (XAFS) analyses of Ni species trapped in graphene sheet of carbon nanofibers. Physical Review B: Condensed Matter, 2006, 73: 144103/1–11
2. Yokoyama A, Sato Y, Nodasaka Y, et al. Biological behavior of hat-stacked carbon nanofibers in the subcutaneous tissue in rats. Nano Letters, 2005, 5: 157–161
3. Sato Y, Shibata H. Kataoka S, et al. Strict preparation and evaluation of water-soluble hat-stacked carbon nanofibers for biomaedical application and their high biocompatibility: Influence of nanofiber-surface functional groups on cytotoxicity. Molecular Biosystems, 2005, 1: 142–145
4. Watari F, Tamura K, Yokoyama A, et al. Biochemical and pathological responses of cells and tissue to micro- and nanoparticles from titanium and other materials. In: Bauerlein E. Handbook of Biomineralization. Weinheim. Wiley-VCH, 2007, 3: 127–144
5. Kumazawa R, Watari F, Takashi N, et al. Effects of Ti ions and particles on cellular function and morphology of neutrophils. Biomaterials, 2002, 23: 3757–3764
6. Tamura K, Takashi N, Kumazawa R, et al. Effects of particle size on cell function and morphology in titanium and nickel. Materials

Transactions, 2002, 43: 3052–3057
7. Watari F, Inoue M, Akasaka T, et al. Comparison of morphology and behavior of carbon nanotubes and asbestos. Proceedings of the 6th Asian BioCeramics Symposium, 2006, 142–145
8. Kiura K, Sato Y, Yasuda M, et al. Activation of human monocytes and mouse splenocytes by single-walled carbon nanotubes. Journal of Biomedical Nanotechnology, 2005, 1: 359–364
9. Sato Y, Yokoyama A, Shibata K, et al. Influence of length on cytotoxicity of multi-walled carbon nanotubes against human acute monocytic leukemia cell line THP-1 *in vitro* and subcutaneous tissue of rats *in vivo*. Molecular BioSystems, 2005, 1: 176–182
10. Yokoyama A, Gelinsky M, Kawasaki T, et al. Biomimetic porous scaffolds with high elasticity made from mineralized collagen—an animal study. Journal of Biomedical Materials Research Part B Applied Biomaterials, 2005, 75B: 464–472
11. Gelinsky M, Bernhardt A, Eckert M, et al. Biomaterials based on mineralised collagen an artificial extracellular bone matrix. In: Watanabe M, Okuno O. Interface Oral Health Science. Japan. Springer, 2007, 323–328
12. Li X M, van Blitterswijk C A, Feng Q L, et al. The effect of calcium phosphate microstructure on bone-related cells *in vitro*. Biomaterials, 2008, 29: 3306–3316
13. Liao S, Wang W, Uo M, et al. A three-layered nano-carbonated hydroxyapatite/collagen/PLGA composite membrane for guided tissue regeneration. Biomaterials, 2005, 26: 7564–7571
14. Liao S, Watari F, Zhu Y, et al. The degradation of the three layered nano-carbonated hydroxyapatite/collagen/PLGA composite membrane *in vitro*. Dental Materials, 2007, 23: 1120–1128
15. Liao S, Xu G, Wang W, et al. Self-assembly of nano-hydroxyapatite on multi-walled carbon nanotubes. Acta Biomaterialia, 2007, 3: 669–675
16. Wang W, Watari F, Omori M, et al. Mechanical properties and biological behavior of carbon nanotube/polycarbosilane composites for implant materials. Journal of Biomedical Materials Research Part B Applied Biomaterials, 2007, 82: 223–230
17. Rosca I D, Watari F, Uo M, et al. Oxidation of multiwalled carbon nanotubes by nitric acid. Carbon, 2005, 43: 3124–3131
18. Aoki N, Akasaka T, Watari F, et al. Carbon nanotubes as scaffolds for cell and effect on cellular functions. Dental Materials Journal, 2007, 26: 178–185
19. Aoki N, Yokoyama A, Nodasaka Y, et al. Cell culture on a carbon nanotube scaffold. Journal of Biomedical Nanotechnology, 2005, 1: 402–405
20. Aoki N, Yokoyama A, Nodasaka Y, et al. Carbon nanotubes deposited on titanium implant for osteoblast attachment. Journal of Bionanoscience, 2007, 1: 14–16
21. Akasaka T, Watari F, Sato Y, et al. Apatite formation on carbon nanotubes. Materials Science and Engineering C, 2005, 26: 675–678
22. Akasaka T, Watari F. Nano-architechture on carbon nanotube surface by biomimetic coating. Chemistry Letters, 2005, 34: 826–827
23. Li X M, Gao H, Uo M, et al. Effect of carbon nanotubes on cellular functions *in vitro*. Journal of Biomedical Materials Research Part A, 2008, DOI: 10.1002/jbm.a.32203
24. Li X M, Gao H, Uo M, et al. Maturation of osteoblast-like Saos2 induced by carbon nanotubes. Biomedical Materials, 2009, DOI: 10.1008/17486041/4/1/015005

Transactions of the Materials Research Society of Japan 33[2] 209-214 (2008)

Reaction of cells and tissue to material nanosizing

Fumio Watari*, Saori Inoue, Noriyuki Takashi, Yasunori Totsuka and Atsuro Yokoyama
Graduate School of Dental Medicine, Hokkaido University, Sapporo 060-8586, Japan
Fax: 81-11-706-4251, e-mail: watari@den.hokudai.ac.jp

Micro/nanosizing effect of materials onto biological organism was investigated by both in vitro biochemical cell functional test and in vivo animal implantation test. Dependence of reaction of cells and tissue, and that of bone formation of apatite on particle size were studied. The increase of specific surface area causes the enhancement of chemical reactivity and therefore toxicity in many cases. This is the most usually and easily recognizable and strongest effect in most cases. However there is the other effect which becomes prominent especially for biocompatible materials such as Ti and TiO_2. Stimulus was increased with the decrease of particle size and pronounced below 3 μm by inducing phagocytosis to cells and inflammation to tissue. For the size below 50nm, particles invade into the internal body through the respiratory or digestive system and diffuse inside body. For bone, synthetic hydroxyapatite exhibits excellent osteoconductivity but it is not substituted with natural bone and remains permanently in the body. When the composite with collagen and nanoapatite synthesized in the biomimetic aspects is implanted, resorption of nanocomposite through phagocytosis by osteoclasts and new bone formation by osteoblasts occurred simultaneously after inflammation. Nanocomposite leads to the bone substitutional properties, which resembles the remodeling process in natural bone. Thus nanosizing induces the intrinsic functions of biological organism and results in the conversion of functions such as from biocompatibility to stimulus and from osteoconductivity but non-bone substitutional to bone substitutional properties through biological process.

Key words: nanosizing, biomaterial, tissue regeneration, inflammation, nanotoxicology, titanium, apatite

1. INTRODUCTION

One of the important fields of nanotechnology is biomedical application. DDS (Drug Delivery System) is one of the most typical bioapplications of nanoparticles. It is well-known that the specific surface area is increased with the decrease of particle size and chemical reactivity is pronounced. Nanosizing effect related to the ionic dissolution which affects on biocompatibility is usually interpreted from this aspect. On the other hand corrosion-resistent and biocompatible Ti causes inflammation in abraded fine particles [1, 2] which are produced from artificial joint, and asbestos [3], a kind of clay minerals, induces mesothelioma after a long-term, large quantity of exposure. These phenomena can be understood as the physical size and shape effect, apart from the material properties of either toxicity or biocompatibility.

On the other hand, hydroxyapatite (HAP), the main component of bone, has the difference in behavior between synthetic apatite and bone. Synthetic hydroxyapatite, in the usual case, of a macroscopic size, exhibits excellent osteoconductivity. However it is not substituted to natural bone and remains permanently in the body. Natural bone is composed of collagen and nanocrystallites of apatite with the size of approximately 50nm. Bone is continuously remodeled by resorption and new bone formation. Thus there exist apatites with the different behavior, non-resorbable and resorbable apatite.

These strongly suggest the necessity to reveal the micro/nanosizing effect of materials onto living organism [4]. In the present study both biochemical cell functional test and animal implantation test were done to clarify the micro/nanosizing effect and particle size dependence of reaction of cells and tissue [5, 6]. The behavior of invasion of nanoparticles and internal diffusion inside body was visualized using XSAM (X-ray Scanning Analytical Microscope) [7, 8] for the level of the whole body and organs. Then the nanosizing effect in apatite was investigated using biomimetic bone-resembling nanoapatite/collagen composite and the mechanism of the different behavior from macroscopic apatite was discussed.

2. EXPERIMENTAL PROCEDURE

Both biochemical cell functional tests and animal implantation tests were done using the fine particles of 99.9% pure Ti, Fe, Ni and TiO_2 for the various sizes from 300 nm to 150 μm [5,6]. Human neutrophils were used as probe cells for various cell toxicity tests, after mixed with particles in HBSS (Hank's balanced salt solution) at 37°C. Histological investigations were done after implanted in the subcutaneous connective tissue of rats.

The compulsory exposure test to the respiratory system was performed using 30nm TiO_2 particles. The

experiments of internal diffusion was done for the particles Ti, Fe, Ni, Pt, TiO_2, TiC, Fe_2O_3 by injection to caudal vein. XSAM observation for the whole body and each organ was conducted in air without the pretreatments of fixation, dehydration and staining after sectioning.

Hydroxyapatite-collagen composites were synthesized biomimetically on mineralized collagen type I. They have the three-dimensional scaffold structures with the interconnecting pores. They were implanted into the subcutaneous tissue and bone defects made in the femur of rats for 1-12 weeks and observed histopathologically [9].

3. RESULTS

Fig.1 shows the comparison of tissue reaction to the macroscopic size (1 mm ϕ x 10 mm) of Ni (a) and Ti (b) after 1 week implantation in the dorsal thoracic region of rat. Implant had been situated in the upper space of each photograph. In Ni the expansion of capillary vessels was observed. Tissue in the photograph was in necrosis and in degeneration in the distant region. For Ti fibrous connective tissue was already formed surrounding implant from the earlier stage, which is the feature of biocompatible materials [10].

Fig.2 showed the tumor occurrence in the subcutaneous tissue of rat after 1 year implantation of 500nm Ni particles. Ni is already toxic in a macroscopic size as seen in Fig.1. When it becomes fine particles, toxicity is enhanced remarkably. This is the typical example of specific surface effect which increases reciprocally to particle size and leads to the enhancement of chemical dissolution and therefore toxicity.

Fig.3 shows the morphology of one of the asbestos (crocidolite: so-called blue asbestos) observed by SEM. The diameter of asbestos is a few nm to a few μm and the length is ranged from submicron to tens of μm. Crocidolite has a distinctly straight needle shape.
There are also very fine particles which may easily disperse as dust.

Asbestos is a kind of clay minerals and silicate in composition. The dissolution level is very low. It is known that asbestos induces mesothelioma after a long-term, large quantity of exposure to respiratory system. This is the result by the different mechanism from that occurred in Ni particles of Fig.2 and related more to the particle size and shape.

Fig.4 shows the histological observation of the reaction of rat soft tissue to the macroscopic Ti implant (a) and 3μm Ti particles (b) after 8 weeks, comparatively. The macroscopic size of Ti implant was surrounded by fibrous connective tissue layer which is the usual reaction for the biocompatible materials. For 3μm Ti numerous inflammatory cells appear. The

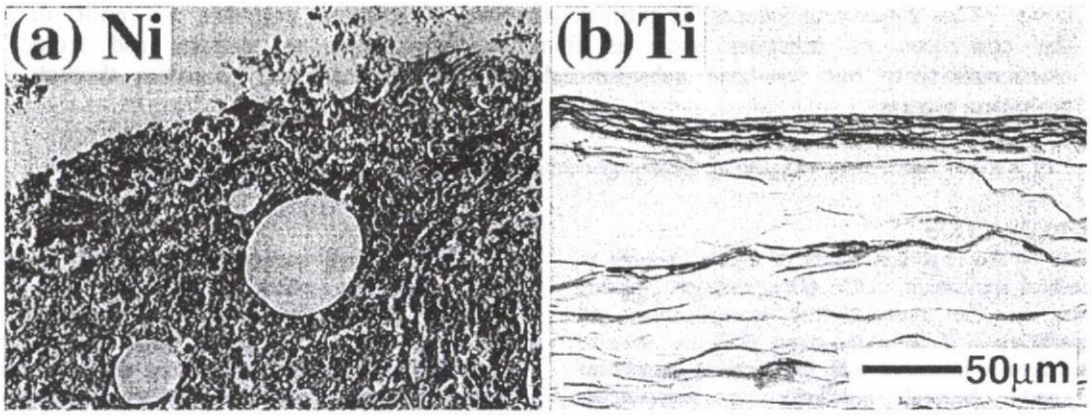

Fig.2 Tumor induced after 1 year implantation of 500nm Ni particles [4].

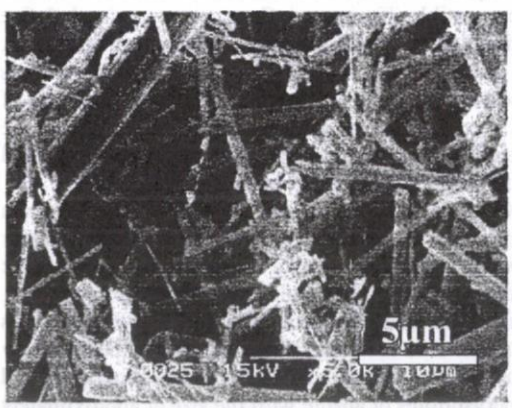

Fig.3 Morphology of asbestos (crocidolite: blue asbestos) observed by SEM.

macrophages and adjacent collagen show degenerative changes in morphology. Ti particles, observed as small black dots, were phagocytized into the cytoplasm by a macrophage.

Fig.5 shows the dependence of superoxide production from human neutrophils on Ti particle size , Superoxide was increased with the decrease of particle size. The increase was pronounced for 3μm and 500nm. The release of LDH and cytokines TNF-α and Il-1ß showed the similar behavior as superoxide, while cell survival rate showed the inverse decreasing tendency. Under these conditions ICP elemental analysis indicated that the dissolution from Ti particles was negligible below detection limit [5].

Fig.6 shows the SEM image of a human neutrophil exposed to 500nm Ti particles in HBSS. The neutrophil is extending its pseudopod and going to phagocytize a 500nm Ti particle. For the particles larger than about 10μm, phagocytosis was not observed. The pronounced phenomena of biochemical cell reaction for below 10μm in Fig.5 are closely related to the phagocytosis shown in Fig.6.

The histological image of in vivo tissue reaction of rat to the different size of Ti particles showed the similar size dependence to those in vitro shown in Figs.5 and 6.

Fig.7 shows the dependence of TNF-α release from neutrophils on particle size down to nm size. TNF-α is one of the most representative cytokines related to inflammation. Stimulus, represented as amount of TNF-α release, which is pronounced below 3μm, exhibited the maximum from around .μm down to 500nm and then for further smaller size decreased below 200nm. This means that the biophylactic system does not work well any more against the invasion of nanoparticles into the inside of body.

Fig.8 is the Ti mapping of the internal whole body of rats by XSAM after compulsory exposure test to respiratory system, and shows the distribution of 30nm TiO_2 particles. The condensation occurred from the respiratory system to urinary bladder by diffusion in the body through the cardiovascular system after the direct uptake into blood vessels from lung cells.

Fig.9 shows the X-ray transmission image and the corresponding Ti elemental mapping by XSAM for 5min and 3hr after injection of 30nm TiO_2 particles to caudal vein. TiO_2 nanoparticles diffused to lung just after injected, then liver and spleen with time course.

Fig.10 is the dental implant composed of hydroxyapatite-coated titanium. Apatite has excellent biocompatibility and induces new bone formation to its surface after implanted in the bone circumstances.

Synthetic hydroxyapatite in the usual case, that is, in

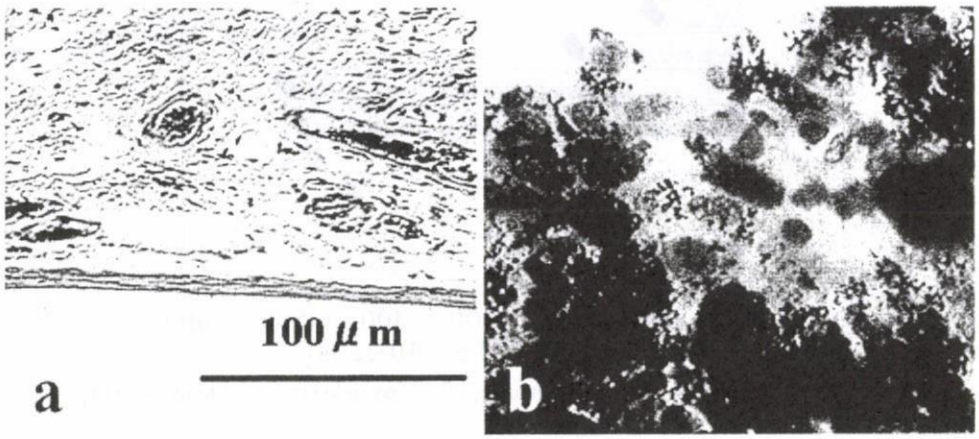

Fig.4 Comparison of reaction of rat soft tissue to the macroscopic Ti implant (a) and 3μmTi particles (b) in histological observation.

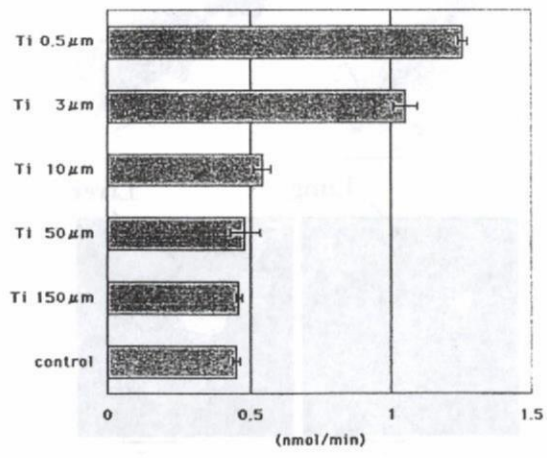

Fig.5 Dependence of superoxide production from neutrophils on Ti particle size [6]

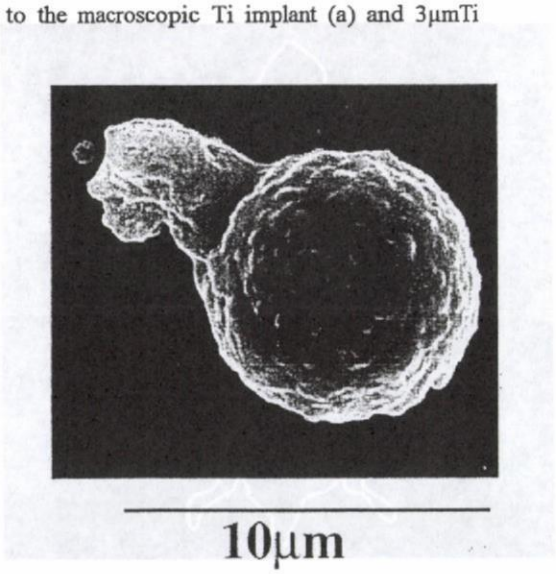

Fig.6 SEM image of a human neutrophil exposed to 500nm Ti particles [6].

a macroscopic size, exhibits excellent osteoconductivity. However it is not substituted to natural bone and remains permanently in the body, therefore it is suitable for the use as implant.

On the other hand it is well-known that natural bone is composed of collagen and nanocrystallites of apatite with the size of approximately 50nm. Fig.11 is the SEM photographs, comparing the difference of morphology of hydroxyapatite for sintered synthetic apatite (a) and natural hard tissue, in this case, enamel of molar of rat (b). In synthetic apatite the size of particles is a few microns and they agglomerate at random, while in enamel enamel prizm of about 5 μm is composed of a bunch of apatite crystallites of about 50nm. It is known that apatite crystallites are grown in their c-axis along collagen fibrils. Thus natural hard tissue is regarded as a kind of composite with the preferably oriented structure of nanocrystallites.

Fig.12 shows the comparison of morphology of hydroxyapatite synthesized without (a) and with (b) collagen by SEM observation. The particle size of apatite is mostly a few microns for without-collagen, while under the coexistence of collagen the product becomes the agglomerate of apatite crystallites of less than 100nm with the lower crystallinity, as revealed from X-ray diffraction analysis.

When the biomimetic nanocomposites of apatite and collagen fibrils were implanted in the subcutaneous tissue, they were covered with fibrous connective tissue and then resorbed mostly at 8 weeks by phagocytosis.

Fig.13 shows the histopathological image when nanocomposites were implanted in the bone marrow of rat for 8 weeks. The area of nanocomposites (asterisks) was decreased and covered with new bone (white asterisks) of lamellar structures. Resorption of the nanocomposites and replacement by new bone proceeded. This tendency was progressed with time by 12 weeks. Phagocytosis of nanoapatite by osteoclasts and osteogenesis by osteoblasts occurred adjacently each other. Resorption and remodeling were similar to the case of autologous bone graft. As a result nanoapatite composites work as bone substitute materials for

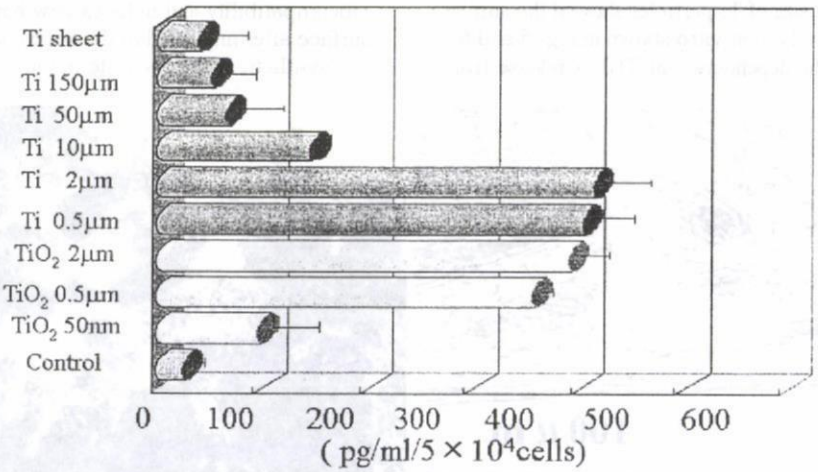

Fig.7 Dependence of TNF-α release from neutrophils on particle size down to nm size [4]

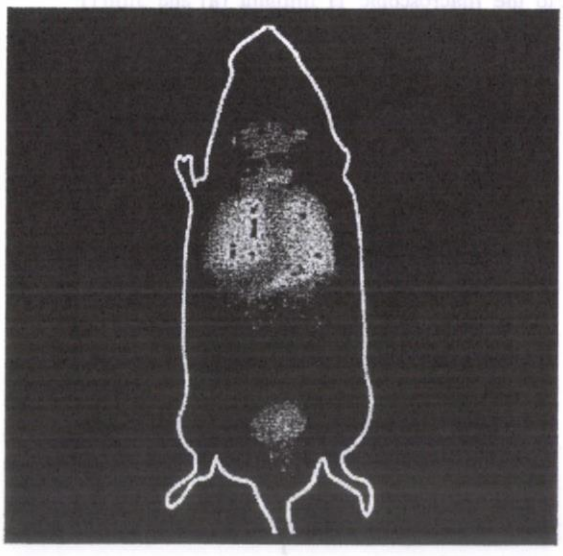

Fig.8 XSAM Ti mapping of internal distribution of 30 nm TiO_2 particles after compulsory exposure test [4].

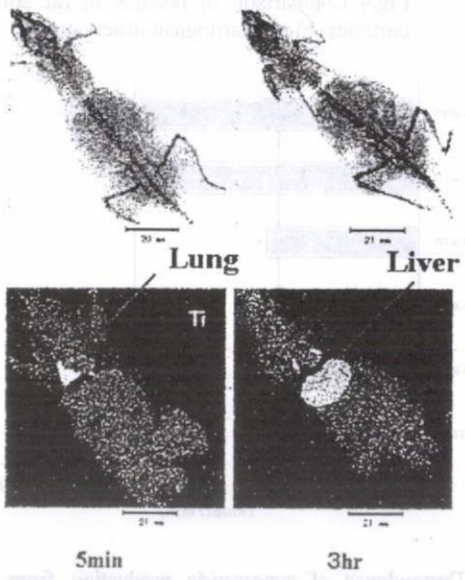

Fig.9 Time course of internal diffusion of 30nm TiO_2 particles after injection to caudal vein

hard-tissue reconstruction.

4. DISCUSSION

4.1 Specific surface area effect and physical particle size effect by nanosizing

Nanosizing effect is usually interpreted in the aspects of the increase of specific surface area. Since chemical reactivity is pronounced with the decrease of particle size, effects related to the ionic dissolution, dominant on biocompatibility of macroscopic materials, accelerate toxicity such as in Ni which generated tumor in the long term implantation for 500nm particles as shown in Fig.2. This effect has the most serious influence, toxicity in many cases, and most commonly taken into account for nanosizing effect. There are, however, other kind of effects. Biocompatible Ti causes inflammation in abraded fine particles [1,2,11], and asbestos [3], a kind of clay minerals, induces

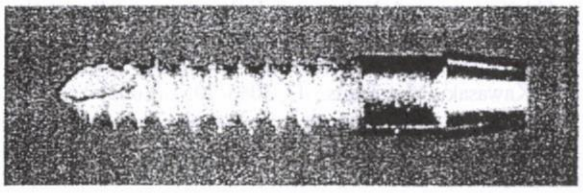

Fig.10 Dental implant composed of apatite-coated titanium

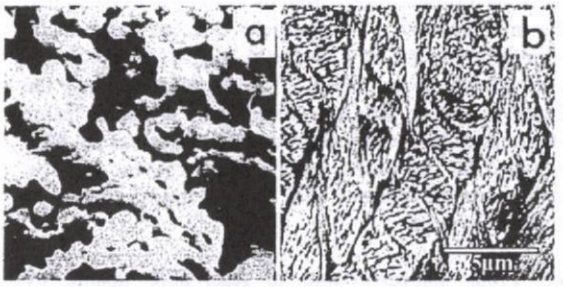

Fig.11 Difference of morphology of hydroxyapatite. a) sintered synthetic apatite, b) enamel of molar of rat.

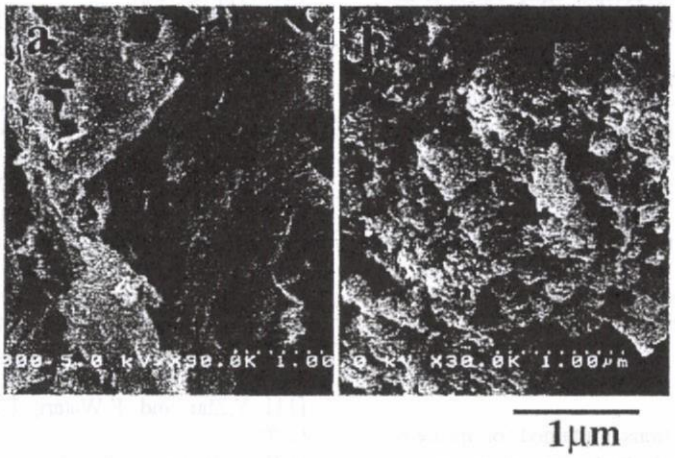

Fig.12 Hydroxyapatite synthesized without (a) and with (b) collagen.

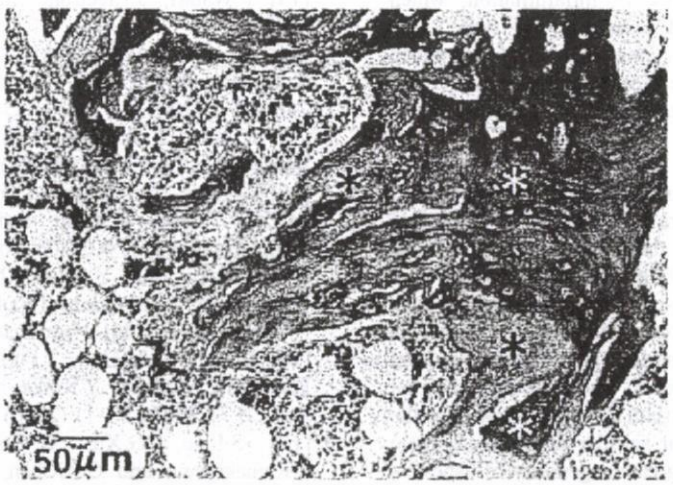

Fig.13 Histological image at 8 weeks after implantation in the bone marrow of rat. Materials (asterisks) were decreased and covered with new bone (white asterisks) with lamellar structures [9].

mesothelioma after a long-term, large quantity of exposure. These phenomena can be understood as the physical particle and shape effect, apart from the material properties of either toxicity or biocompatibility. Particles below 10 μm cause phagocytosis to cells and inflammation to tissue even for biocompatible materials such as Ti and TiO_2.

4.2 Invasion of nanoparticles into internal body

By compulsory exposure test, the 30nm TiO_2 particles diffuse directly from the respiratory system into the internal body. Nanoparticles injected from caudal vein diffused with time course to lung, liver and spleen. The uptake of the 30nm TiO_2 particles through the digestive system. was also confirmed. Particles below 50nm might be the objects whose existence has not been assumed by the living body defense system and can invade into the internal body through the respiratory or digestive system.

4.3 From non-resorbable to resorbable apatite by nanosizing

Synthetic hydroxyapatite exhibits excellent osteoconductivity in a macroscopic size, but it is not substituted to bone and remains permanently in the body, therefore it is suitable for the use as implant [12]. It is well-known that natural bone is composed of collagen and nanoapatite crystallites of approximately 50nm [13]. When the biomimetically synthesized nanoapatite composite with collagen [9,14] is implanted, phagocytosis and inflammation is induced. Osteoclasts and osteoblasts are then differentiated. Phagocytosis by osteoclasts and new bone formation by osteoblasts is simultaneously activated and proceeded as shown in Fig.13. As a result, nanoapatite composite leads to the bone substitutional properties.

4.4 Induction of bioactive properties and conversion of functions by nanosizing

The conversion of functions is attained for apatite by nanosizing - from osteoconductivity in macroscopic size to bone substitutional properties in nano/micro scale. Nanoparticles cause the reaction of cells/tissue and stimulate to the occurrence of inflammation, which works as toxicity in most cases and, for some cases depending on the situation, pronounces the conversion of functions leading to the bioactive properties. Nano structure is essential for these stages to be processed.

5. CONCLUSIONS

Nanosizing of materials induces the reaction of cells and tissue and the intrinsic functions of biological organism, which leads to the conversion of functions such as from biocompatibility to stimulus and from osteoconductivity but non-bone substitutional to bone substitutional properties through biological process. This is different from specific surface area effect originated solely from material properties. There are controversial arguments as to whether carbon nanotubes may have the serious toxicity due to their acicular or fibrous particle shape, associated with lung carcinogenicity of asbestos, whilst we have rather found the favorite properties as biomaterials [15-19]. The physical particle size and shape effect in micro/nanosizing is the essential basis for the proper understanding of such phenomena and for the development of biomedical applications of nanotechnology.

6. ACKNOWLEDGEMENTS

The present study was performed under the support of Health and Labour Sciences Research Grants in Research on Chemical Substance Assessment from the Ministry of Health, Labour and Welfare of Japan (H18-Chemistry-General-006).

REFERENCES

[1] Y.Tamura, A.Yokoyama, F.Watari and T.Kawasaki, Dental Materials J., 21, 355-372 (2002)
[2] Y.Tamura, A.Yokoyama, F.Watari, M.Uo and T.Kawasaki, Mat.Trans., 43, 3043-3051 (2002)
[3] F.Watari, M.Inoue, T.Akasaka, N.Sakaguchi, H.Ichinose and M.Uo, Proc.6th Asian BioCeramics Symp.2006, 142-145 (2006)
[4] F.Watari, K.Tamura, A.Yokoyama, K.Shibata, T.Akasaka, B.Fugetsu, K.Asakura, M.Uo, Y.Totsuka, Y.Sato and K.Tohji, "Handbook of Biomineralization, Vol.3", Ed. by E.Bauerlein, Wiley-VCH, Weinheim (2007) pp127-144
[5] R.Kumazawa, F.Watari, N.Takashi, Y.Tanimura, M.Uo and Y.Totsuka, Biomaterials, 23, 3757-3764 (2002)
[6] K.Tamura, N.Takashi, R.Kumazawa, F.Watari and Y.Totsuka, Mat.Trans., 43 , 3052-3057 (2002)
[7] M.Uo, F.Watari, A.Yokoyama, H.Matsuno and T.Kawasaki, Biomaterials, 20, 747-755 (1999)
[8] M.Uo, M.Tanaka and F.Watari, J.Biomed.Mater.Res., Part B:Appl.Biomater., 70B, 146-151 (2004)
[9] A.Yokoyama, M.Gelinsky, T.Kawasaki, T. Kohgo, U.König, W.Pompe and F.Watari, J. Biomed Mater Res Part B:Appl Biomater, 75B, 464-472 (2005)
[10] H.Matsuno, A.Yokoyama, F.Watari, M.Uo and T.Kawasaki, Biomaterials, 22, 1253-1262 (2001)
[11] Y.Zhu and F.Watari, Dent.Mat.J., 26, 245-253 (2007)
[12] F.Watari, A.Yokoyama, M.Omori, T.Hirai, H.Kondo, M.Uo and T.Kawasaki, Composites Science and Technology, 64, 893-908 (2004)
[13] F.Watari, J.Electron Microscopy, 54, 299-308, (2005)
[14] S.Liao, W.Wang, M.Uo, S.Ohkawa, T.Akasaka, K.Tamura, F.Cui and F.Watari, Biomaterials, 26, 7564-7571 (2005)
[15] N.Aoki, T.Akasaka, F. Watari and A.Yokoyama, Dent.Mat.J., 26, 178-185 (2007)
[16] N.Aoki, A.Yokoyama, Y.Nodasaka, T.Akasaka, M.Uo, Y.Sato, K.Tohji and F.Watari, J.Biomed. Nanotechnology, 1, 402-405 (2005)
[17] A.Yokoyama, Y.Sato, Y.Nodasaka, S.Yamamoto, T.Kawasaki, M.Shindoh, T.Kohgo, T.Akasaka, M.Uo, F.Watari and K.Tohji, Nano Letters, 5, 157-161 (2005)
[18] M.Ushiro, K.Uno, T.Fujikawa, Y.Sato, K.Tohji, F.Watari, W.Chun, Y.Koike and K.Asakura, Phys. Rev., B 73, 144103/1-11 (2006)
[19] S.Liao, G.Xu, W.Wang, F.Watari, F.Cui, S.Ramakrishna and C.K.Chan, Acta Biomaterialia, 3, 669–675 (2007)

(Recieved September 5, 2007 ; Accepted March 26, 2008)

特集 ナノ粒子材料とその安全性

ナノ粒子の生体反応性と為害性発現

材料のサイズがマクロからミクロ,ナノに微小化したときの効果として代表的なものは比表面積増大効果による化学反応の活性化であるが,これとは別に生体との相互作用に基づく微粒子特有の効果も現れる.これらは人間の意図する目的と合致すれば高機能性というメリットとして作用するが,一方また意図せずして為害性というデメリットとして発現する可能性もある.マクロとは異なり,ナノ粒子は本質的に高機能性と刺激性の二面性を併せ持つことを認識する必要がある.

亘理　文夫

生体に対する材料と微粒子の効果とは？

栄養摂取にせよ毒性発現にせよ，材料と生体との相互作用の多くは水溶性としてイオン化して体内に吸収されることから開始する．可溶性のNaは容易に摂取され摂取過剰になることもあるのに対し，難溶性のCaは吸収されにくい．試薬のカタログを見るとBa化合物のほとんどが劇物・毒物といったラベルがしるされているにもかかわらず，硫酸バリウムのみなにも記されず胃カメラで用いられるのは溶解度がきわめて低いからであろう．結婚式の食事で出て来るスープに金粉がちりばめられていることがあるが，健康に問題ないのだろうか．純金であればイオン化傾向が最も小さく，イオン溶出が無いと見なせるから，消化器を単に通過するだけであれば，何事も起きないであろう．このようにマクロでの材料の生体適合性には溶出性（だけではない）が，大きな影響を及ぼす．この傾向はミクロ/ナノになっても変わらない．コーヒーへの角砂糖と粉末状の砂糖の溶けやすさからも明らかのように，微粒子になりサイズが小さくなると，比表面積は増大するから，溶解性や化学反応性は著しく増大する．この効果は目に見えて大きく，多くの場合，微粒子化またはミクロ/ナノサイズ化（以下ナノサイジングとも記載）の効果はこの比表面積効果で説明されている．この効果は生体と無関係に生ずる材料の効果である（図1）[1]．

しかしナノサイジング効果はこれだけに留まらない．生体親和性にすぐれるチタンが人工関節骨頭摺動部で使用され，摩耗粉となると周囲組織に炎症を起こし骨融解を導いて使用寿命が10年程度になる場合があることや，粘土鉱物の１種アスベストを長期大量に被曝すると中皮腫を発症する現象には，単に材質が毒性か生体親和性かという特性とは別に，微粒子という物理的サイズに起因する効果が寄与していると考えられる[2]．

ここではまず，マクロでもアレルギー性等の為害性を呈するNiを溶出性金属の代表として，生体親和性[3]に富みインプラント[4]に多く使用されているTiを非溶出性の代表的金属として取り上げ，マクロからミクロ/ナノへ微小化したときの生体

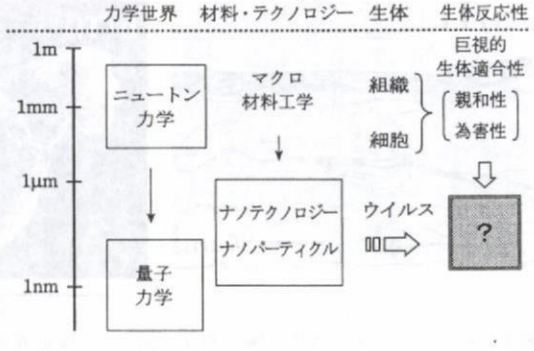

図1　ナノテクノロジーの力学世界，生体との関係，および材料のマイクロ/ナノサイジングと生体反応性の関連

反応性を比較して見てみよう．

ミクロ/ナノ粒子化と生体反応

図2はマクロサイズの材料に対する生体軟組織の反応（in vivo組織埋入試験），図3は微粒子化（0.5μm）したときの個々の細胞に対する反応（in vitro細胞毒性試験），図4はこの微粒子を軟組織に長期埋入した結果（in vivo）である[5]．

図1では直径1mmの棒状インプラントをラット皮下軟組織に1週埋入後の周囲組織の一部で，図の上部に挿入されていたインプラントは取り除かれている．Niでは組織が壊死し，強い為害作用を示すが，Tiではインプラントを被包化する線維性結合組織が形成されており，生体親和性に富む材料の典型的な反応を示している．

材料がμm程度の微粒子になると細胞は図3のように，Niに対しては強い為害性のために細胞は破壊され，Tiでは貪食が誘発されている．ここで用いた細胞のヒト好中球は白血球の約50％を占める5～10μmと比較的小さな顆粒球で，生体内の異物に対して非特異的に反応する貪食細胞の一種である[6) 7)]．

この条件下で各微粒子からのイオン溶出量をICP（誘導結合プラズマ）元素分析すると，Ti微粒子では検出限界値以下であり，イオン溶出は無視できると考えられる．即ち，Ti微粒子に対する反応は物理的サイズ・形状に由来する効果である[6) 7)]．

これらの微粒子を大量に半年～1年間軟組織に埋入すると（図4），Niでは腫瘍が発生し，Tiでは貪食を繰返し微粒子群が次第に凝集する中，慢性的な炎症が継続する．

物理的サイズ効果の特徴

溶出性材料における比表面積効果は図3(a)，図4(a)のように作用が顕著で認識しやすい．一方，そうした化学的溶出効果が無視し得る非溶出性材料やbioactive, bioinert材料でもμm～nmになると，材質によらず微粒子の物理的サイズ効果による刺激性が顕現化する（図3(b)，図4(b)）．

図5は微粒子と共在させたヒト好中球から産生したサイトカインTNF-αの微粒子サイズ依存性を示したものである（in vitro細胞機能性試験）[2)]．サ

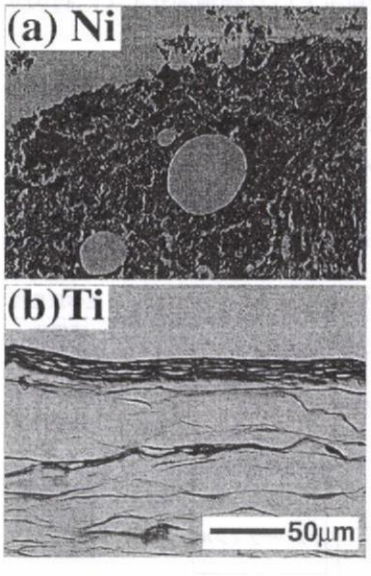

図2　マクロサイズの各種金属に対する軟組織の反応（ラット皮下埋入1週後）．(a) Ni, (b) Ti

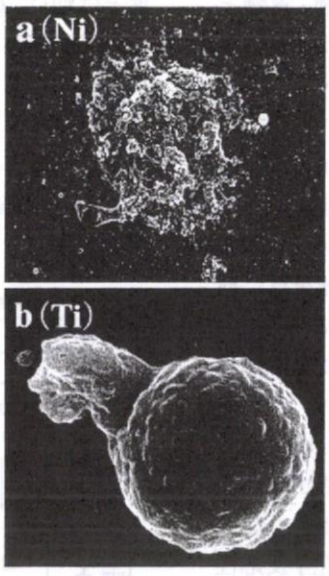

図3　各種金属微粒子に対するヒト好中球の反応（SEM像）．(a) Ni (0.5μm), (b) Ti (0.5μm)

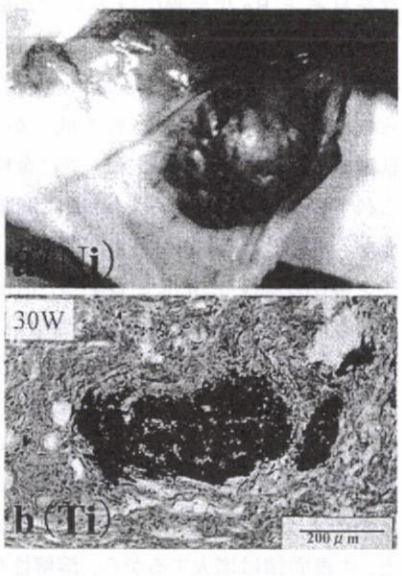

図4　ラット軟組織に長期（6ヵ月～1年）埋入後の各種金属微粒子に対する反応．(a) Ni (0.5μm), (b) Ti (0.5μm)

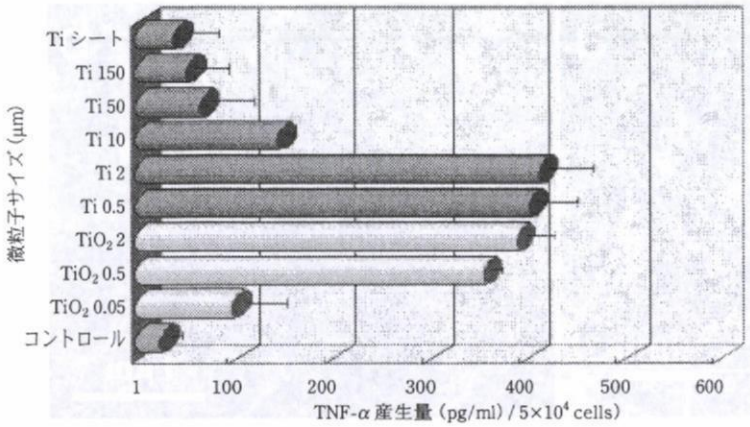

図5　炎症性サイトカインTNF-α産生の微粒子サイズ依存性

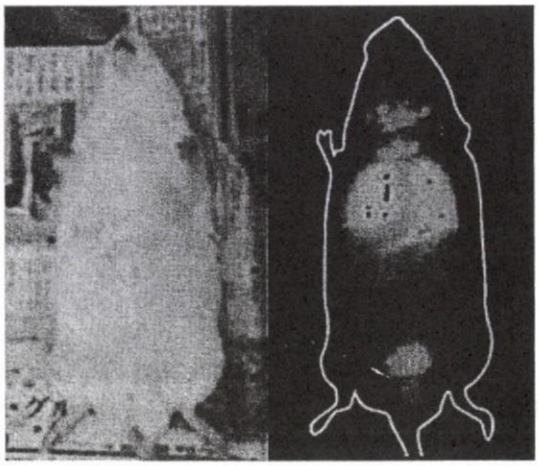

図6　呼吸器系からのナノ微粒子の体内侵入/全身拡散：30nmTiO_2粒子の強制露曝試験後のXSAMマッピングによるラット体内の全身Ti元素分布像[5]．

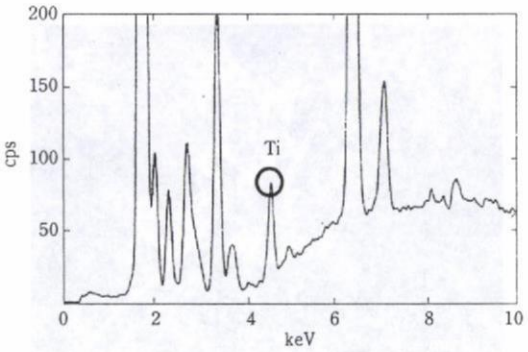

図7　消化器系からのナノ微粒子の体内取込/全身拡散：30nmTiO_2粒子を10日間投与後の脾臓からのX線元素分析．Tiが検出される[11]．

イトカインは細胞から放出される比較的低分子量の蛋白質で細胞間のシグナル伝達，新たな細胞の分化・誘導等の機能を果たしている．サイトカインは多数存在するが，TNF-αは代表的な炎症性サイトカインの一種で，刺激性や炎症の程度を示す指標と考えることができる．Ti微粒子サイズが150μmから0.5μmへ順次小さくなるにつれ，放出量は増加する傾向にあるが，とりわけ10μm以下になると急激に増加している．

in vitro, in vivo試験の結果を総合すると，100μm以上では巨視的サイズと同様の親和性を示すが，50μm以下では刺激性が亢進し，特に10μm以下になると細胞に貪食（図3(b)）を誘発して，刺激性が増大し（図5），組織に炎症（図4(b)）を引き起こす現象が金属，セラミックス，ポリマー共通に起きる．これは微粒子と細胞・組織との相対的なサイズの大小関係に由来し，生物学的プロセスによって非特異的に刺激性を示現する効果である（図1）．

ナノ粒子の体内侵入・全身拡散

この材料に非特異的な物理的粒子サイズに由来する刺激性は，μm近傍で最大値を示した後，さらに小さくなりnm領域になるとむしろ低下する（図5）[2]．ナノ物質の応用の観点からは一見都合がよさそうに見えるが，別の見方をすれば異物に対する生体の認識能力あるいは防御能力が低下するということにも通ずる．

微粒子の大きさが約10μmを切ると気管支を通過するが，図6は化粧品に使われている30nmの

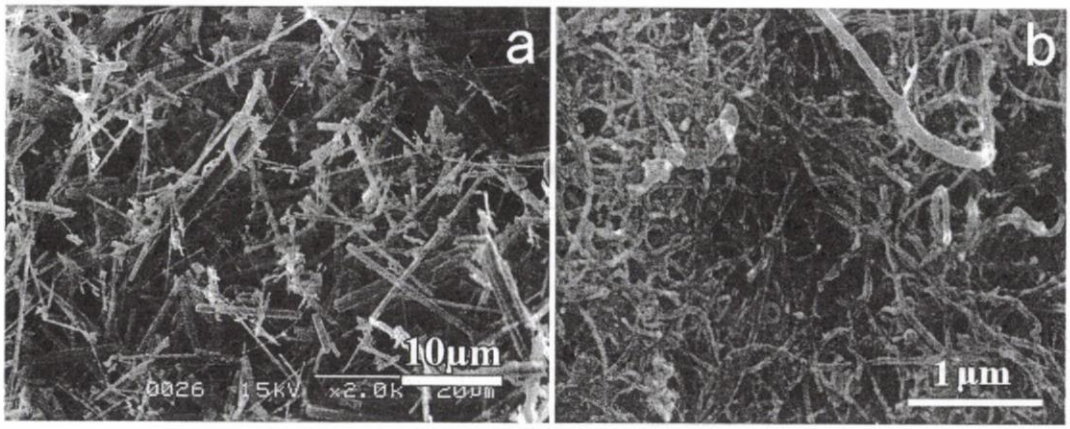

図8　(a) アスベスト (クロシドライト：青石綿) と (b) カーボンナノチューブの粒子形態[5]

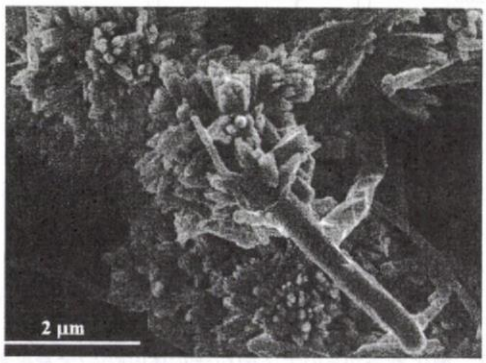

図9　人工体液浸漬によるカーボンナノチューブへのアパタイト析出

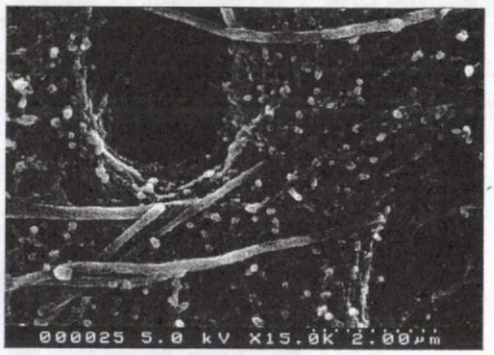

図10　脱灰象牙質表面に露出したコラーゲン線維へのカーボンナノチューブの吸着

TiO_2粉末をラットに強制曝露試験したときのX線走査型分析顕微鏡 (XSAM)[8)~10)] によるTi元素分布像である[5]. 呼気にのって肺胞に到達したナノ粒子が肺から直接血中に取り込まれ，全身に拡散することがわかる.

図7は同じ粒子を10日間経口投与後，脾臓から取得したX線元素分析スペクトルである. Tiが検出されており，消化器系からも体内侵入・全身拡散を起こすことが示される[11].

カーボンナノチューブとアスベスト

カーボンナノチューブは主として電子エミッター，燃料電池など電子，化学分野で注目され，応用開発がなされている. 欧米からは肺ガン誘発性のあるアスベストとの形状の類似性 (図8)[5] の連想から重大な為害性があるという論調が出されていた[12]. しかしそれに相当する実際のデータは無いままに，議論されてきたところがあるが，最近，発癌しやすいラットを使用して中皮に直接曝露する腹腔内埋入試験により，中皮腫が発生したという報告が出された[13]. 長期大量に被爆した場合，アスベストと同様な発癌性を呈するかについては，カーボンナノチューブ[14] には様々なものがあり，また特性や挙動がアスベストとは異なる面があり[15]，今後なお検討を要するが，その為害性の有無如何に関わらず，生産現場等，長時間大量に扱う環境では，被曝を避ける予防的措置を取ることは当然必要である.

カーボンナノチューブのバイオ応用に注目した研究は今日に至るまできわめて少ないが，筆者らの行った細胞機能性試験[16)17)]，動物埋入試験[18)] か

らは，bioinert材料一般に起きる程度の微粒子刺激性は有するものの，短中期的には特異的な生体為害性は認められず[19]，むしろ生体材料として有利な細胞・組織に対する特徴的な種々の親和性が多数見出され，バイオ用カーボンナノチューブの開発[20]，糖鎖・アパタイトによる表面修飾，組織再生用スカフォールド等[21]，バイオ応用へ向けた開発を行っている．図9はカーボンナノチューブを人工体液に浸漬した際に生ずるアパタイトの析出，図10は酸で脱灰した歯の象牙質部の表面に露出したコラーゲン線維に，蛋白質や糖鎖への親和性に富むカーボンナノチューブが吸着する例である．

おわりに

健康と環境問題は，2008年7月に開催されたG8北海道洞爺湖サミットでも取り上げられたように，21世紀に直面する主要課題である．ナノテクノロジーの進展とともに，ナノ物質の開発が進行し，新しい機能性や高効率化が実現されつつあるが，一方，ナノサイズ化により化学反応は著しく促進されることから，メリット（高機能性）とともに，意図せずしてデメリット（為害性）もまた昂進される可能性がある．これらはしかし人間にとって有効か逆効かという価値判断に依存した評価であり，同一種の現象の表裏の関係にあると言える．

例えば抗癌剤を投与するとしばしば癌患部に到達する前に健常組織に吸収され体力を損なう副作用に働いてしまうが，DDS（ドラッグデリバリーシステム）はその欠点を回避するために，癌患部にのみ特異的に結合する修飾基を付けて血流中を移送し薬剤を投与しようとするナノ粒子の代表的なバイオ応用例である．こうした薬物体内動態は意図的に血液に投与した作用であるのに対し，図6に示したナノ粒子の体内侵入・全身拡散[22]は意図せずして血中を回流する効果であって，人間の目的にかなうか否かの違いだけで現象的には全く同一である．

2000年以来，筆者らはほぼ世界に先駆け，材料のミクロ/ナノサイジングに対する生体反応性を調べ，ナノテクノロジーの人体へのバイオ応用にはあらかじめ起こり得る生体反応と条件を把握する必要があるということをデータに基づき繰返し提起してきた．またその中でカーボンナノチューブのバイオ応用性も見出してきた．しかしこうした話題はナノテクのイメージに対してマイナスであるとして必ずしも好まれないところがある．

ナノ微粒子は生体防御機構が想定していない対象である可能性があり，高機能性と刺激性の両面を併せ持ち，その制御が重要であるということを基本的な認識として持つ必要がある．アスベストの二の轍を踏むことのないよう，産業労働衛生[23]や地球環境保全の観点からナノテクノロジーのリスクアセスメントもまた国民の安心できるナノテク開発の確立のために必須である[24]．

通常，ナノテク関連の学会は応用性を追求するがリスク評価のテーマは好まれず，トキシコロジー（毒性）分野では為害性のみ強調する傾向があり，両極に分かれがちである．筆者らはナノテクノロジーのバイオ医用応用と安全性評価の両者を同一の場で検討することを意図し，研究会を開催してきたが[25]，この種の会議は世界的にも類例がなく，今後，機会を得て学会設立へと発展させたいと考えている．

繰返しになるが，ナノ物質の有害性発現はナノ物質の生体反応性から言えばその一局面に過ぎず，材料の微細化に伴う生体反応自体はきわめて興味深く本質的な研究分野である．

例えば骨の主成分はリン酸カルシウムの一種ハイドロキシアパタイトであるが，我々の骨の構造はナノアパタイトから成る複合材料と見なすことができ，骨吸収と形成のプロセスを繰返すリモデリングを常に行っている．実際マクロな人工アパタイトはすぐれた骨伝導性を示すが，骨に置き換わらないのに対し，生体を模倣したナノアパタイトーコラーゲン/コンポジットを骨欠損部に埋入すると，骨置換性に機能性転換する[26]．こうした現象はナノ微粒子であるから生物学的プロセスにおいて可能なのであり，ナノ構造は生体に必須とも言うことができる[27]．

参考文献

1) 亘理文夫：バイオマテリアル－生体材料－ **24** (5), (2006), 300-310.

2) F.Watari, K.Tamura, A.Yokoyama, K.Shibata, T.Akasaka, B.Fugetsu, K.Asakura, M.Uo, Y.Totsuka, Y.Sato, K.Tohji: Handbook of Biomineralization Vol.3, Ed.E.Bauerlein, Wiley-VCH, Weinheim, (2007), p.127-144.

3) H.Matsuno, A.Yokoyama, F.Watari, M.Uo, T.Kawasaki: Biomaterials, **22** (2001), 1253-1262.

4) F.Watari, A.Yokoyama, M.Omori, T.Hirai, H.Kondo, M.Uo, T.Kawasaki: Composites Science and Technology, **64** (6) (2004), 893-908.

5) F.Watari, S.Abe, C.Koyama, S.Inoue, T.Akasaka, M.Uo, M.Matsuoka, N.Takashi, Y.Totsuka, E.Hirata, A.Yokoyama, M.Esaki, M.Morita, T.Yonezawa: Proc. ISNST, 2007 (2007), p.43-52.

6) R.Kumazawa, F.Watari, N. Takashi, Y.Tanimura, M.Uo, Y.Totsuka: Biomaterials, **23** (2002), 3757-3764.

7) K.Tamura, N. Takashi, R.Kumazawa, F.Watari, Y.Totsuka: Mat. Trans., **43** (12) (2002), 3052-3057.

8) M.Uo, F.Watari, A.Yokoyama, H.Matsuno, T.Kawasaki: Biomaterials, **20** (8) (1999), 747-755.

9) M.Uo, F.Watari, A.Yokoyama, H.Matsuno, T.Kawasaki: Biomaterials, **22** (2001), 1787-1794.

10) 亘理文夫：日本歯科医師会雑誌, **51** (12) (1999), 1199-1208.

11) F.Watari, S.Abe, K.Tamura, M.Uo, A.Yokoyama, Y.Totsuka: Bioceramics Vol.20 Part 1, (Key Engineering Materials Vols.361-363), Trans. Tech. Publ., (2007), p.95-98.

12) 松田正己：現代化学 2005 年 12 月号（通巻 417 号), (2005), 14-16.

13) A.Takagi, A.Hirosea, T.Nishimura, N.Fukumori, A.Ogata, N.Ohashi, J.Kanno: J.Toxical. Sci. **33** (1) (2008), 105-116.

14) M.Ushiro, K.Uno, A.Fujikawa, Y.Sato, K.Tohji, F. Watari, Wang-Jae Chun, Y.Koike, K.Asakura: Physical Review, **B 73** (2006), 144103/1-11.

15) F.Watari, M.Inoue, T.Akasaka, N.Sakaguchi, H.Ichinose, and M.Uo: Proc. 6th Asian BioCeramics Symp., (2006), 142-145.

16) K.Kiura, Y.Sato, M.Yasuda, B.Fugetsu, F.Watari, K.Tohji, K.hibata: J.Biomed. Nanotechnology, **1** (2005), 359-364.

17) Y.Sato, A.Yokoyama, K.Shibata, Y.Akimoto, S.Ogino, Y.Nodasaka, T.Kohgo, K.Tamura, T.Akasaka, M.Uo, K.Motomiya, B. Jeyadevan, M.Ishiguro, R. Hatakeyama, F. Watari, K. Tohji: Molecular BioSystems, **1** (2005), 176-182.

18) A.Yokoyama, Y. Sato, Y. Nodasaka, S.Yamamoto, T.Kawasaki, M. Shindoh, T.Kohgo, T. Akasaka, M.Uo, F.Watari, K.Tohji: Nano Letters, **5** (1) (2005), 157-161.

19) 亘理文夫：ナノカーボンハンドブック，エヌ・ティー・エス, (2007), p.887-893.

20) Y.Sato, . Shibata, H. Kataoka, S. Ogino, B.Fugetsu, A. Yokoyama, K. Tamura, T.Akasaka, M.Uo, K.Motomiya, B.Jeyadevan, R.Hatakeyama, F.Watari, K.Tohji : Molecular Bio Systems, **1** (2005), 142-145.

21) N. Aoki, T.Akasaka, F. Watari, A.Yokoyama : Dent. Mat. J., **26** (2) (2007), 178-185.

22) F.Watari, S.Abe, C.Koyama, A.Yokoyama, T.Akasaka, M.Uo, M.Matsuoka, Y.Totsuka, M.Esaki, M.Morita, T. Yonezawa: J.Ceram. Soc. Jap., **116** (1) (2008), 1-5.

23) 亘理文夫：ナノ粒子の有害性評価とリスク対策，技術情報協会, (2007), p.436-449.

24) 亘理文夫：バイオマテリアル－生体材料－ **24** (4), (2006), 235-236.

25) 亘理文夫（編者）：「ナノトキシコロジーアセスと微粒子・ナノチューブのバイオ応用」研究会抄録集，第1回（H17/12/12，仙台）(2005), p.1-35/第2回（H18/6/22-23, 札幌）(2006), p.1-45/第3回（H18/12/11-12，仙台）(2006), p.1-33/第4回（H19/8/1, 東京）(2007), p.1-35/第5回（H19/12/18, 名古屋）(2007), p.1-38/第6回（H20/6/16-17, 札幌） Int. Symp. on "Nanotoxicology Assesment and Biomedical, Enviromental Applocation of Fine Particles and Nanotubes (ISNT2008)", (2008), p.1-78.

26) A.Yokoyama, M.Gelinsky, T.Kawasaki, T.Kohgo, U. Konig, W.Pompe, F.Watari: J. Biomed Mater Res Part B: Appl Biomater, **75B** (2005), 464-472.

27) F.Watari, A.Yokoyama, M.Gelinsky, W.Pompe: Interface Oral Health Science 2007, Ed. M.Watanabe, O.Okuno: Springer Japan (2008), 139-147.

わたり・ふみお　WATARI Fumio

1976 東京大学大学院工学系研究科修了，ベルギー原子力研究所，アントワープ大学，アリゾナ州立大学，東北大学科学計測研究所，東京医科歯科大学を経て，1993～ 北海道大学大学院歯学研究科教授．専門：生体材料学，バイオイメージング，ナイトキシコロジー／ナノバイオ応用開発．